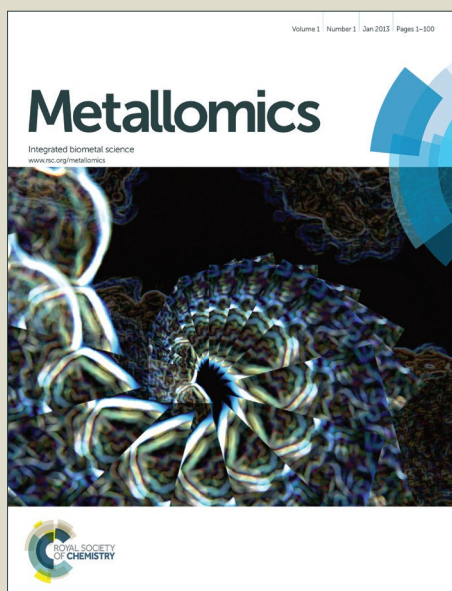


Metallomics

Accepted Manuscript



This is an *Accepted Manuscript*, which has been through the Royal Society of Chemistry peer review process and has been accepted for publication.

Accepted Manuscripts are published online shortly after acceptance, before technical editing, formatting and proof reading. Using this free service, authors can make their results available to the community, in citable form, before we publish the edited article. We will replace this *Accepted Manuscript* with the edited and formatted *Advance Article* as soon as it is available.

You can find more information about *Accepted Manuscripts* in the [Information for Authors](#).

Please note that technical editing may introduce minor changes to the text and/or graphics, which may alter content. The journal's standard [Terms & Conditions](#) and the [Ethical guidelines](#) still apply. In no event shall the Royal Society of Chemistry be held responsible for any errors or omissions in this *Accepted Manuscript* or any consequences arising from the use of any information it contains.



Metallomics

ARTICLE

Interaction of mercury and selenium in the larval stage zebrafish vertebrate model

Received 00th January 20xx,
Accepted 00th January 20xx

DOI: 10.1039/x0xx00000x

www.rsc.org/

Tracy C. MacDonald,^{abc} Malgorzata Korbas,^{cd} Ashley K. James,^{abc} Nicole J. Sylvain,^c Mark J. Hackett,^a Susan Nehzati,^a Patrick H. Krone,^{cd} Graham N. George^{*abe} and Ingrid J. Pickering,^{abe}

The compounds of mercury can be more toxic than those of any other non-radioactive heavy element. Despite this, environmental mercury pollution and human exposure to mercury are widespread, and are increasing. While the unusual ability of selenium to cancel the toxicity of mercury compounds has been known for nearly five decades, only recently have some aspects of the molecular mechanisms begun to be understood. We report herein a study of the interaction of mercury and selenium in the larval stage zebrafish, a model vertebrate system, using X-ray fluorescence imaging. Exposure of larval zebrafish to inorganic mercury shows nano-scale structures containing co-localized mercury and selenium. No such co-localization is seen with methylmercury exposure under similar conditions. Micro X-ray absorption spectra support the hypothesis that the co-localized deposits are most likely comprised of highly insoluble mixed chalcogenide $\text{HgS}_x\text{Se}_{(1-x)}$ where x is 0.4–0.9, probably with the cubic zincblende structure.

Introduction

The compounds of mercury are more toxic than any other non-radioactive element,¹ but despite its toxicity mercury exposure of humans is surprisingly widespread. Mercury in the environment can be divided based upon its chemistry into inorganic forms, comprising elemental Hg and Hg^{2+} compounds, and organometallic forms, comprising methylmercury CH_3Hg —and related compounds. Sources of exposure to inorganic mercury include the burning of fossil fuels, the use of mercury-containing dental restoratives, and the practice of artisanal gold mining procedures in parts of the developing world.^{3,4} Sources of methylmercury exposure are primarily through consumption of marine fish,^{4,5} particularly large predatory species such as swordfish or shark, which have high methylmercury contents.

Both inorganic and organometallic forms of mercury are highly toxic, but with quite distinct toxicologies.^{1,2} Inorganic mercury is neurotoxic, and can also give rise to kidney damage, digestive tract problems, increased blood pressure, altered heart rate, and acrodynia.¹ Organic mercury compounds are also neurotoxic, but are typically more potent in this regard than inorganic mercury, targeting the central nervous system. While adults can be severely affected by organic mercury,

infants are especially sensitive, particularly when exposed *in utero*.¹ Despite its toxicity, and its potential to adversely impact human health, many unanswered questions remain about the mechanisms of mercury's toxicity and the extent of human health risk from exposure.

The toxicology of mercury has been known to be linked to the biochemistry of selenium for nearly five decades.⁶ Since the initial reports, the protective effects of selenium administration have since been studied extensively, both in animal models^{7,8} and more recently in human brain.⁹ In all previous animal studies of the interaction of mercury and selenium, organisms were dosed both with compounds of mercury and with compounds of selenium,⁸ whereas in the study of human exposure only endogenous selenium is implicated.⁹

Larval stage zebrafish (*Danio rerio*) are increasingly used as a model vertebrate in toxicology. Their advantages include high fecundity, well characterized developmental stages, and genomic characterization.¹⁰ Previously we have used the larval zebrafish model in combination with X-ray fluorescence imaging (XFI)¹¹ in the study of mercury toxicology for both organic and inorganic forms.^{2,12–14} We present herein an XFI and micro-X-ray absorption spectroscopy (μ -XAS) study of the interaction of both inorganic and organic forms of mercury with endogenous selenium in the zebrafish model.

Experimental

Zebrafish

All procedures were approved by the University of Saskatchewan Ethics Board. Embryos were collected, rinsed, and raised to 72 hours post fertilization (hpf) in methylene blue (to prevent fungal growth) with system water (1 mL methylene

^a Molecular and Environmental Science Research Group, Department of Geological Sciences, University of Saskatchewan, Saskatoon, SK, S7N 5E2, Canada. E-mail: g.george@usask.ca

^b Toxicology Centre, University of Saskatchewan, Saskatoon, SK, S7N 5B3, Canada

^c Department of Anatomy and Cell Biology, University of Saskatchewan, Saskatoon, SK, S7N 5E5, Canada

^d Canadian Light Source, 44 Innovation Boulevard, Saskatoon, SK, S7N 2V3, Canada

^e Department of Chemistry, University of Saskatchewan, Saskatoon, SK, S7N 5C9, Canada

blue: 1 L system water) in a 28°C incubator with a 14:10 h light:dark cycle. By 72 hpf zebrafish larvae had hatched from their chorions and were exposed to either system water (control), 2 μM HgCl_2 , or 0.5 or 1 μM CH_3HgCl . Preliminary studies on 20-ID-D used 24-36 h exposures to 2 μM HgCl_2 and 1 μM CH_3HgCl . Subsequent studies used 48 h exposures, but with a lower CH_3HgCl dose of 0.5 μM in order to prevent morbidity. In all cases doses were chosen based on our previously reported studies² so as to prevent larval morbidity and mortality.

Zebrafish were rinsed three times then embedded in JB-4 methacrylate as previously described.² Zebrafish larvae to be imaged at Advanced Photon Source (APS) beamline 20-ID-B and at the Stanford Synchrotron Radiation Lightsource (SSRL) beamline 2-3 were sectioned to 6 μm thick and mounted on Thermanox plastic coverslips (Gibco BRL). For imaging at APS beamlines 2-ID-D and 2-ID-E, 3 μm thick sections were collected and mounted on 500 nm thick silicon nitride windows (Silson Ltd., Northampton, England). In most cases, trunk sections (Fig. 1) were scanned to interrogate a variety of tissues and organs in a single section.

X-ray Fluorescence Imaging (XFI)

XFI data were collected at the APS with the storage ring containing 102 mA at 7 GeV in top-up mode on beamlines 20-ID-B, 2-ID-D and 2-ID-E. Additional XFI data collection and X-ray absorption spectroscopy were carried out at SSRL with the storage ring operating at 500 mA at 3 GeV on beamline 2-3. All beamlines employed Si(111) double crystal monochromators with Rh-coated mirrors employed for focusing and harmonic rejection at the APS. On APS 20-ID and SSRL 2-3, micro-focus X-ray beams of respective approximate diameters of 5 and 2 μm were obtained by using Rh-coated Kirkpatrick-Baez mirrors, with samples mounted at 45° to the incident X-ray beam. The high-resolution micro-focused beams on 2-ID-D and 2-ID-E were generated by Fresnel zone plates (X-radia, Pleasanton, CA). In all cases an incident X-ray energy of 13.45 keV was selected to be above both the Se K-edge and the Hg L_{III} edge, but below the Br K-edge to avoid unwanted Br fluorescence from plastic components of the experimental setup. X-ray fluorescence was monitored using silicon-drift Vortex detectors (Hitachi High-Technologies Science America Inc., Northridge, CA, USA). Data reduction and analysis were carried out as previously described.^{2,9,12-15} Following established practices¹¹ we quantify mercury, selenium and other elements as areal densities a which are normally expressed in units of $\mu\text{g}/\text{cm}^2$. A conversion to equivalent concentration in mM can be accomplished by computing $a \times 10^4 / (tM)$ where t is the sample thickness in μm and M is the molecular weight.

Micro X-ray absorption spectroscopy (μ -XAS)

Micro-XAS data were recorded on SSRL beamline 2-3 using the setup as described for XFI. Following XFI, the beam was positioned on the cells of the pronephric duct. To obtain data approaching adequate signal to noise, 28 spectra of 20 minutes each were averaged. Spectra were calibrated with reference to a Hg-Sn amalgam, assuming the lowest energy inflection of the L_{III}

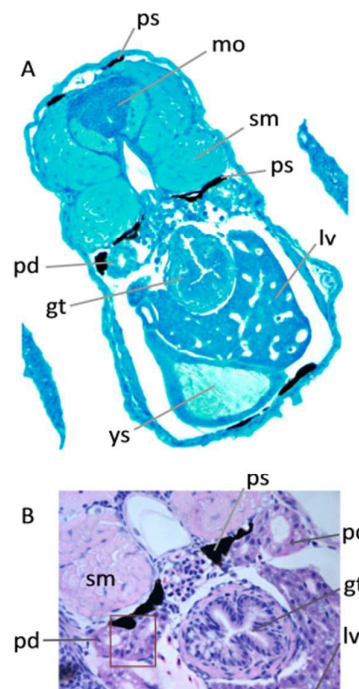


Fig. 1 Typical larval zebrafish trunk sections, stained with methylene blue (A) and hematoxylin and eosin (H&E) (B). A shows the whole section indicating hindbrain (medulla oblongata; mo), somitic muscle (sm), pronephric ducts (pd), liver (lv), gut tube (gt), pigment spots (ps) and yolk sac (ys). B shows a higher resolution micrograph with a typical region of a kidney sections studied at high resolution indicated by the red rectangle, which included both the midline pigment spot and the pronephric ducts.

edge to be 12.285 keV. Data were analyzed using the EXAFSPAK suite of programs.¹⁶

Correlation plots

With correlation plots of XFI data, errors are present in both abscissa and ordinate. Contrary to common practice, the use of standard linear regression is not appropriate for analysis of XFI correlation plots as standard linear regression considers only a single dependent variable, typically graphed on the ordinate, with no presumed errors in abscissa. The resulting line differs depending on whether Hg or Se (for example) is plotted on the abscissa. A valid method for XFI correlation plots is to minimize the sum of the squares of the perpendicular (closest) distance from each point to the line, the slope of which estimates the ratio of the two elements for the data set. A custom computer program was written for this purpose.

Results and discussion

X-ray fluorescence imaging (XFI)

Figure 2 shows selenium and mercury XFI data for trunk sections of zebrafish larvae treated with mercuric chloride and with methylmercury chloride, together with a section from a control fish with no exogenous mercury. The locations of the sections were chosen to show a range of important anatomical features, including the liver, somitic muscle, the hind-brain (medulla

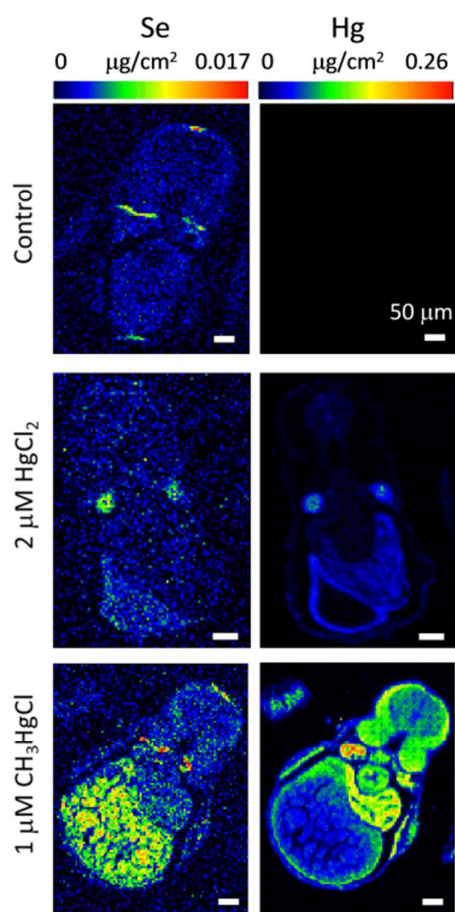


Fig. 2 Localization of selenium and mercury in trunk sections of larval zebrafish exposed to system water (control), 2 μ M HgCl_2 , or 1 μ M CH_3HgCl . Each section was imaged using a step size of 5 μ m and a dwell time of 0.6 s on beamline 20-ID. The levels of Se and Hg are shown as areal density ranges, which correspond to concentration ranges of 0-0.36 mM and 0-2.2 mM for Se and Hg, respectively.

oblongata), the pronephric duct (kidney), the yolk sac, and the gut (Fig. 1). The mercury XFI data show the previously described differences in tissue-specific localization as a function of administered mercury chemical form.² The inorganic mercury treated section shows localization to the kidney and to a lesser extent the liver, whereas the organic mercury treatment shows concentration in organs including the kidney, liver, somitic muscle, gut and brain, as well as some accumulation in the yolk sac, especially at the periphery. As expected the control shows no detectable mercury.

The fish in the present study were not supplemented with selenium in any way. The fish larvae at this developmental stage are not yet feeding so that all of their nutrition, including the selenium observed by XFI, is derived from maternal transfer through the yolk sac. The actual amount of selenium in the yolk sac has been observed to vary from fish to fish, presumably because of variations in maternal transfer.¹⁹ This can be observed in Fig. 2 which shows high Se levels in the yolk sac for the CH_3HgCl exposed larva, but lower amounts in the other sections. Moreover, the other sections in Fig. 2 happen to have less prominent yolk sacs. Selenium in the control section (Fig. 2),

without exogenous mercury, is observed to be localized predominantly in pigmented tissues, which occur most prominently along the midline pigmentation lying between the kidney and somitic muscle (Fig. 1). We have observed previously that pigment spots show high levels of localized zinc.¹⁵ The black pigment of zebrafish is predominantly comprised of melanin and related pigments, synthesized in melanophores. While the association of zinc with melanin has been known for more than six decades,¹⁷ the chemistry of this association remains unexplored. It seems likely that the zinc is coordinated through the oxygen donors of the catechols that are integral to the polymeric melanin, although whether the zinc is adventitious or has some specific function is unknown. Unlike zinc, the association of selenium with pigment has not been reported previously for zebrafish, although we have consistently observed it in the course of previous studies. In contrast, the association of selenium and neuromelanin in human brain has been reported,¹⁸ although the chemical nature of this selenium also remains unknown.

When fish were treated with methylmercury compounds, the selenium distribution appeared similar to the controls which were not treated with exogenous mercury compounds, showing selenium localized most strongly to pigmented areas (Fig. 2). There was no apparent co-localization of selenium with mercury in the fish tissues. In marked contrast, when fish were treated with inorganic mercury (HgCl_2), clear co-localization of exogenously administered mercury with endogenously derived selenium can be seen in the pronephric ducts. In addition, selenium levels in the pigment spots are negligible, suggesting that selenium in these regions may have been depleted in favor of co-localization with mercury in the pronephric ducts. In our XFI data the selenium is present at lower levels than that of mercury, with maximum levels, in the case of kidney, that are about 10% of the observed mercury maxima (Fig. 2). The low levels accumulated can be gauged from the average concentrations over the zebrafish tissues in this section which we compute as 0.084 and 0.33 mM, for Se and Hg, respectively.

Since at the spatial resolution of Fig. 2 (5 μ m) the strong co-localization within the pronephros is in intense spots that appear smaller than 1 pixel, we examined sections at higher spatial resolutions. XFI results using a 500 nm resolution X-ray beam are shown in Fig. 3. As before, the mercury-selenium co-localized areas were only observed with inorganic mercury, and were less than one pixel across. The selenium levels in the pigmented areas, as clearly demarked by the zinc localization in the XFI data, were observed to be depleted (Fig. 3), reinforcing the suggestion that the selenium that is co-localized with mercury originated in the pigmented areas. Figure 4 shows a region scanned at the still higher XFI resolution of 250 nm. Here also the spots were less than one pixel in size, indicating the presence of nano-sized structures less than 250 nm across containing both Hg and Se. However, a single bright spot of mercury in the sample showed much lower accumulation of selenium, indicating chemical heterogeneity. Moreover, the levels of selenium off the co-localized regions were relatively higher than those of mercury indicating either a background

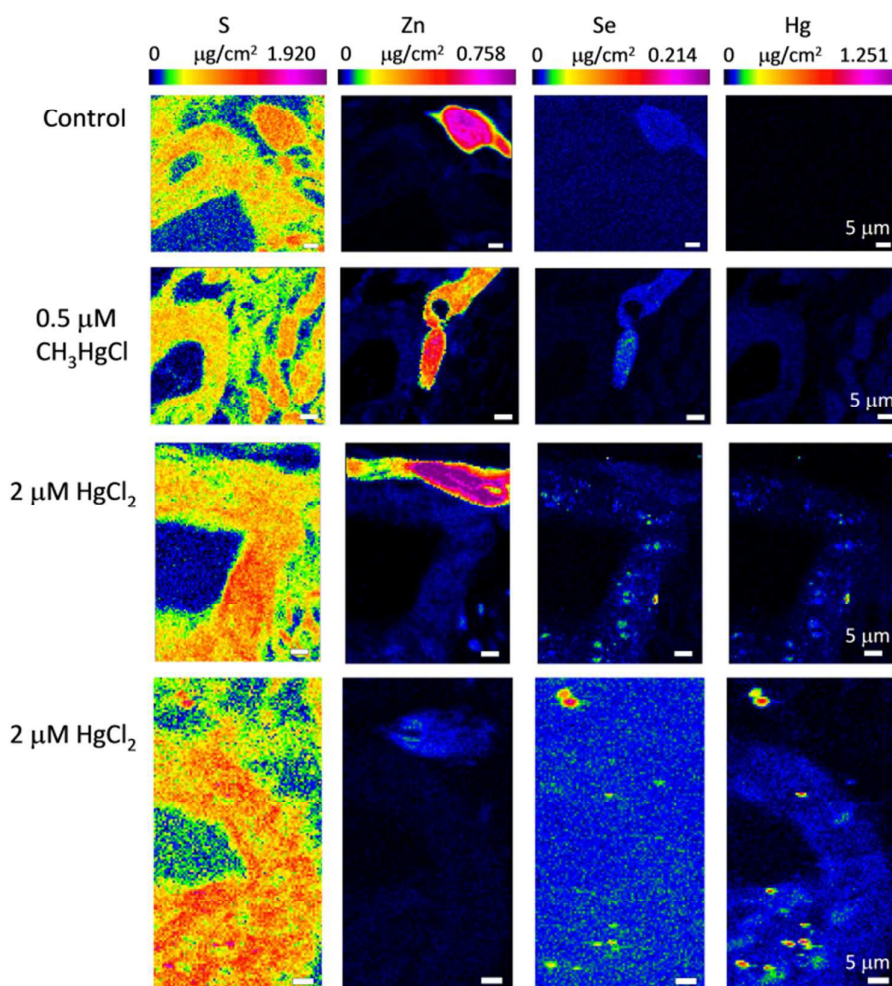


Fig. 3 Localization of sulfur, zinc, selenium, and mercury in pronephros of larval zebrafish exposed to system water (control), 0.5 μM CH_3HgCl , or 2 μM HgCl_2 . Sections were imaged at beamline 2-ID-D and 2-ID-E. A typical section of this region is indicated in Figure 1. The pigment spots can be located by their high zinc content.

tissue level of selenium or an incomplete removal of scattered radiation.

Figure 5 shows a section taken through the eye and brain of a zebrafish larva treated with 2 μM HgCl_2 . In this case the eye lens contains large quantities of selenium, which we have previously observed using confocal methods in selenium supplemented fish,¹⁹ but with the rest of the section showing selenium levels that are more typical of those observed in the trunk section. In particular, pigmented areas of the retina show high relative selenium levels, consistent with those observed in the pigmented areas of the trunk section. Within the brain co-localization of mercury and selenium in small regions is again observed in the fish exposed to inorganic mercury. As with the kidney, mercury is consistently higher than selenium. Figure 6 shows a higher resolution data set of part of the dorsal brain from a larval zebrafish eye section. The epiphysis, the dorsal thalamus, habenula (which plays a role in olfactory perception²⁰) can all be seen in the figure and these, together with surrounding tissues, are peppered with nano-sized deposits of Hg and Se with in this case an Hg:Se molar ratio of about 2-3:1.

Correlations plots

Correlation plots of the levels of Hg and Se for four higher resolution images (Fig. 3, 5 and 6) are shown in Fig. 7. In all cases for HgCl_2 treated larvae, there is excellent correlation between the levels of Hg and Se in the regions of the images with elevated levels. This is best illustrated when data are limited to include only the top 90% of Hg and Se levels, which excludes the pixels with almost no Hg and Se that are close to the axes origin. Using the top 90%, correlation coefficients for all images from HgCl_2 treated larvae are in the vicinity of 0.9 (Fig. 7). For the data from HgCl_2 treated larvae shown in Fig. 7, the slopes of the lines give the Hg:Se mass ratios, in most cases being close to 4:1, corresponding to molar ratios of 1.6:1. In contrast, with the data from methylmercury chloride treated larvae no correlation is seen between Hg and Se, with an R^2 (90%) value of only 0.24.

The other kidney section from a HgCl_2 treated larva (Fig. 3, lower panels) shows a different type of relationship, the correlation plot for which is shown in Fig. 8. Here there are two distinct correlation domains, and subjecting the data to a domain sorting algorithm with regression analysis indicates that

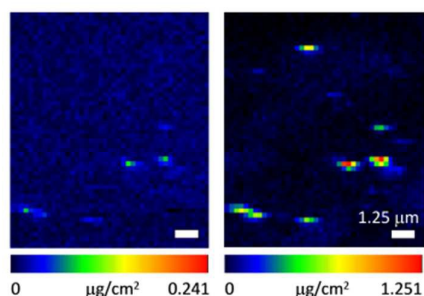


Fig. 4 High resolution XFI of selenium and mercury in zebrafish pronephric duct of the zebrafish exposed to 2 μM HgCl_2 shown in Figure 3. Image collected using a step size of 250 nm and a dwell time of 1 s per pixel on beamline APS 2ID-E.

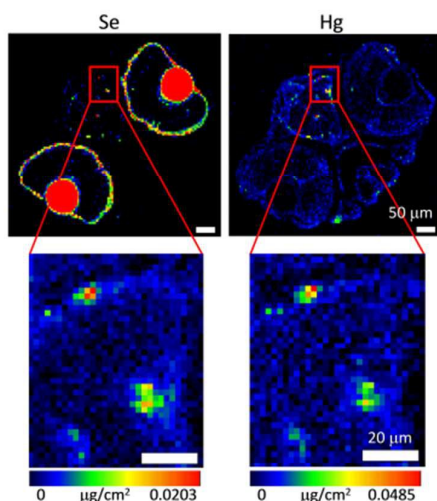


Fig. 5 Mercury selenium co-localization in zebrafish brain of fish exposed to 2 μM HgCl_2 . The upper image of the entire section was imaged on APS 20-ID using a step size of 5 μm and a dwell time of 0.6 s per pixel. The higher resolution image region (indicated with the red box) was collected subsequently using a step size of 2 μm and a count time of 0.6 s per pixel.

two linear relationships exist with slopes of 19 and 4.5, respectively, with respective R^2 (90%) values of 0.89 and 0.97. The respective Hg:Se molar ratios of the two domains correspond to 7.5:1 and 1.8:1. The images corresponding to the

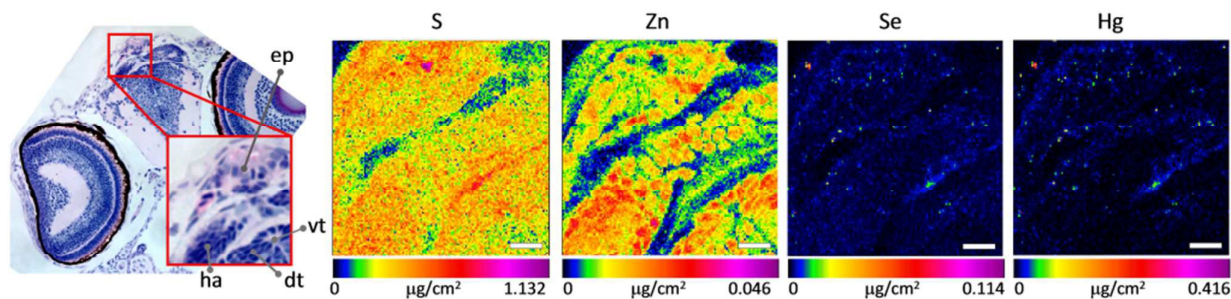


Fig. 6 High-resolution (500 nm) XFI of larval zebrafish brain imaged at APS beamline 2-ID-D. The H&E stained histology of the adjacent section to that scanned with XFI is shown on the left of the figure, with the area scanned outlined as a red rectangle. The epiphysis (ep), habenula (ha), dorsal thalamus (dt) and ventricle (vt) are indicated.

domain-sorted data are also shown in Fig. 8. The higher Hg content domain (the red line in Fig. 8) lies predominantly within the cells of the wall of the pronephric duct itself, whereas the lower Hg domain (the blue line in Fig. 8) lies mostly exterior to the duct. This clearly indicates that the observed Hg:Se ratio is variable and is tissue specific.

In mammals, injection of solutions of sodium selenite and mercuric chloride causes a mutual detoxification through formation of nano-particulate HgSe in blood plasma.⁷ Similar protective effects for different Se compounds with Hg intoxication have also been demonstrated,²¹ including with larval stage zebrafish.²² These particles have an approximate size of 100–200 atoms^{7,23} and may be sequestered by selenoprotein P.²³ Selenoprotein P is the most abundant extracellular selenoprotein and is now known to be important in selenium homeostasis, especially in brain.^{25,26} It seems probable that the reported binding of nano-particulate HgSe ²³ is adventitious, rather than a genuine function of selenoprotein P, and that the sequestration by this essential selenium transporter may indeed be detrimental through diversion of the transporter from its proper function. Indeed, previous work has shown that glutathione can fulfil a similar function by acting as an external ligand to the HgSe nano-particles.⁷ The HgSe nanoparticles forming in blood give XAS spectra that are consistent with the zincblende structure,⁷ in which both Se and Hg are bound to each other in approximately tetrahedral geometries, in agreement with the crystal structure of the bulk HgSe mineral tiemannite.^{27,28} Compounds related to HgSe , such as CdSe , can exist in either zincblende or wurtzite structures, especially when in nanoparticulate form, and as previously discussed these structures cannot be rigorously distinguished using XAS.⁷ Bulk mercuric sulfide (HgS) exists in two stable forms at room temperature. The familiar red form, $\alpha\text{-HgS}$, is thermodynamically favored at ambient conditions and has a structure named for its mineral form, cinnabar, with chains of two-coordinate mercury and sulfur.²⁹ The black form, $\beta\text{-HgS}$, known mineralogically as metacinnabar, is kinetically favored being quite close in energy to $\alpha\text{-HgS}$, and is isostructural with bulk HgSe having the zincblende structure with four-coordinate tetrahedral Hg and S. In mineral formations tiemannite often contains substitution of sulfur for selenium in its structure as the mixed chalcogenide $\text{Hg}_x\text{S}_{1-x}$ with almost the whole range of HgSe to HgS compositions having been observed.³⁰ Synthetic colloidal clusters of $\text{Hg}_x\text{S}_{1-x}$, varying in size between 2 and 3 nm, were

also shown to have the cubic zincblende structure of the bulk.³¹

Micro-X-ray absorption spectroscopy (μ -XAS)

In the zebrafish model we have described co-localizations of Hg and Se that occur with Hg:Se molar stoichiometries that vary from 7.5:1 to 1.6:1. Sulfur is present at high levels throughout the samples (Fig. 3), consistent with its various and diverse biological roles. We note that sample regions containing co-localized Hg and Se also contain elevated levels of sulfur (Fig. 3, Fig. 6). Our data are therefore consistent with the presence of nano-sized particles of the mixed chalcogenide $\text{HgS}_x\text{Se}_{(1-x)}$. In order to investigate this possibility further we used μ -XAS to examine the chemical form of mercury in situ. The results of this for zebrafish pronephric duct are shown in Fig. 9, together with selected model compounds. The mercury L_{III} near-edge spectra show only subtle variation with chemical form, and because of the relatively low overall levels of Hg, the XAS spectra reported here have poorer signal to noise than that normally required for unambiguous speciation.³³ Moreover the even lower levels of selenium meant that collection of Se K-edge spectra with usable signal to noise ratios was not practical for these samples. Nevertheless, comparison of the Hg L_{III} near-edge spectrum with those of standard compounds indicates that the fish spectrum most resembles that of β -HgS, supporting the hypothesis that mercury is sequestered as a mixed chalcogenide $\text{HgS}_x\text{Se}_{(1-x)}$ where x is 0.44–0.87 most probably with the cubic zincblende structure typical of these materials.³¹ Both β -HgS and HgSe are

highly insoluble compounds, with extremely low molar solubility products.³⁴ They can be regarded as essentially chemically inert under biological conditions, with the mercury effectively sequestered and potentially benign. Fish with mercury sequestered in this way lack the typical selenium co-localization in the pigment spots, suggesting that the source of the selenium bound in $\text{HgS}_x\text{Se}_{(1-x)}$ is that associated with the pigment spots in the control. As we have already discussed, this selenium must originate in the yolk sac, but whether it is diverted from its transport from the yolk to the pigment spots and other tissues, or is remobilized from that already in pigment spots and other tissues remains unknown. Selenium is an essential element for all kingdoms of life, with a number of roles in vertebrates including redox homeostasis.³⁵ Irrespective of whether the selenium involved in mercury sequestration is depleted from tissues directly or comes from the yolk, localized depletion of essential selenium in the fish tissues may be in part responsible for the toxic effects of inorganic mercury.³⁶ Indeed, depletion of essential selenium through inhibition of essential selenoenzymes has been suggested as a primary source of mercury's toxicity in what is known as the selenium depletion hypothesis.³⁶

Conclusions

Here we show that endogenous selenium can play a role in vertebrates by sequestering inorganic mercury, probably as the insoluble mixed chalcogenide $\text{HgS}_x\text{Se}_{(1-x)}$. Such sequestration has

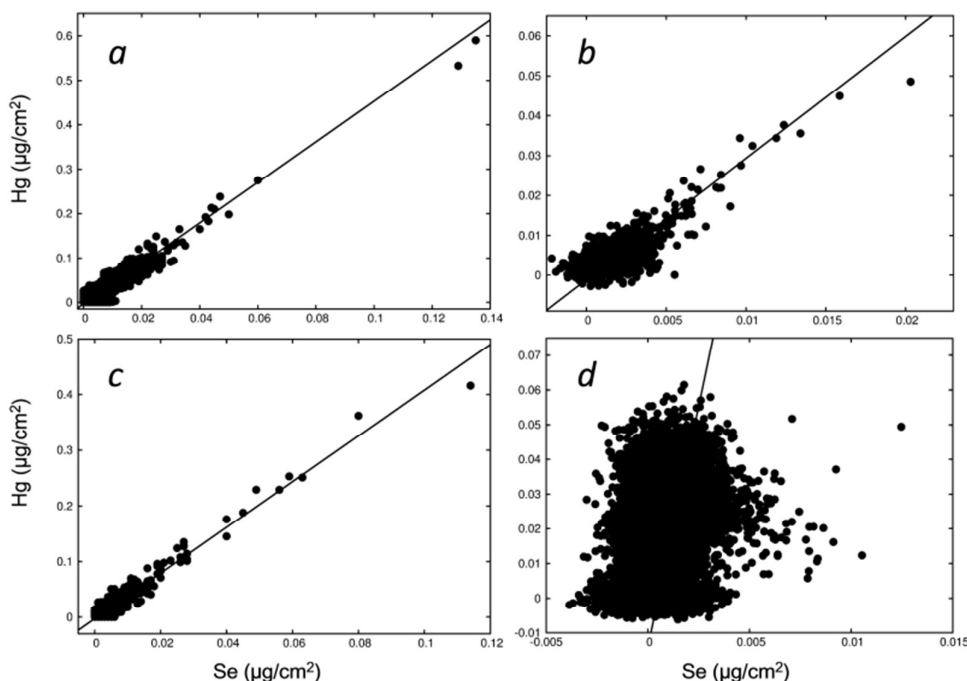


Fig. 7 Correlation plots of Hg vs. Se for selected data sets. *a* shows the kidney section from Fig. 3 with HgCl_2 treatment, *b* and *c* the brain sections with HgCl_2 treatment from Fig. 5 and 6, respectively, and *d* shows the kidney section from CH_3HgCl treated larvae from Fig. 3. The straight lines are derived from regression analysis, as described in the methods section, and give slopes (mass ratios) of 4.6, 3.1 and 4.1 for *a*, *b* and *c*, respectively, with intercepts within 0.005 of the origin in all cases. Correlation coefficients, R^2 , are 0.76 (0.98), 0.53 (0.84) and 0.70 (0.98) for the data from HgCl_2 treated larvae *a*, *b* and *c*, respectively, where the values in parentheses are the R^2 excluding points with less than 10% of maximum. The data from CH_3HgCl treated larvae give R^2 values of 0.12 (0.24) indicating that there is no correlation between Hg and Se in this sample.

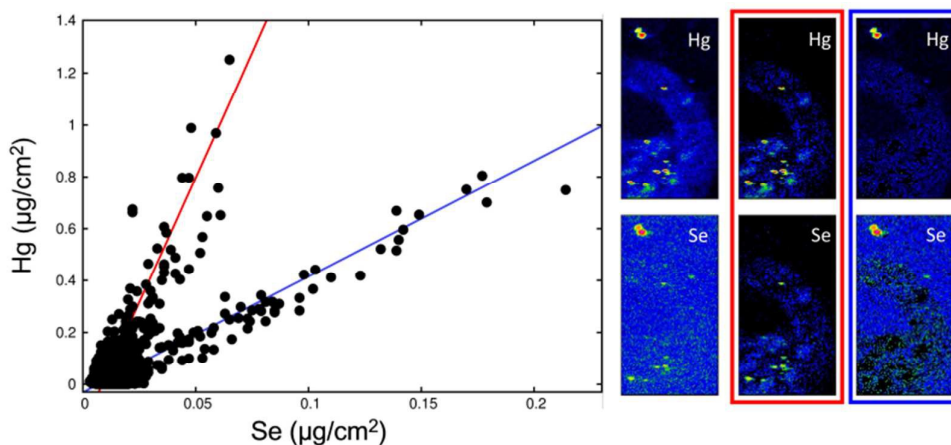


Fig. 8 Correlation plot of Hg vs. Se for a kidney section from a HgCl_2 treated zebrafish showing two distinct correlation domains. The red line shows the domain 1 correlation and the blue line shows the domain 2 correlation. The images display the Hg and Se images with (left to right) total, domain 1 (red outline) and domain 2 (blue outline). The slopes for domain 1 and domain 2 were 19.2 and 4.5, respectively. The correlation coefficients, R^2 , were 0.79 (0.89) and 0.53 (0.97) where the values in parentheses are the R^2 excluding points with less than 10% of maximum.

been suggested to be part of detoxification mechanisms in other vertebrates, including humans, subsequent to *in situ* demethylation of methylmercury compounds.⁹ Our observations are on a much shorter time scale following mercury exposure than previous work,⁹ and under our conditions the rapid formation of mixed chalcogenides $\text{Hg}_x\text{Se}_{(1-x)}$ suggests that inorganic mercury, whether this is the form of initial exposure or from demethylation of methylmercury species, might be sequestered very rapidly in exposed humans. An open question is whether selenium supplementation might also play a prophylactic role in populations exposed to high mercury.

Acknowledgements

We thank members of the George-Pickering research group and beamline staff of APS and SSRL for their assistance. This work was supported by the Canadian Institutes of Health Research (GNG, IJP), the Saskatchewan Health Research Foundation (GNG, IJP), the University of Saskatchewan, and Natural Sciences and Engineering Research Council of Canada Discovery Grants (to PHK, and to IJP). MK was supported by a grant from the Canada Foundation for Innovation and partners (to GNG and IJP) through funding for BioXAS: Life Science Beamline for X-ray Absorption Spectroscopy at the Canadian Light Source. GNG and IJP are Canada Research Chairs. TCM, MJH and SN are CIHR-THRUST Fellows, and MJH is supported by a CIHR post-doctoral fellowship award. This research used resources of the Advanced Photon Source (APS), a U.S. Department of Energy (DOE) Office of Science User Facility operated for the DOE Office of Science by Argonne National Laboratory under Contract No. DE-AC02-06CH11357. Sector 20 facilities at the APS, and research at these facilities, are supported by the U.S. DOE, Office of Basic Energy Sciences (OBES), the Canadian Light Source and its funding partners, the University of Washington, and the APS. Use of the Stanford Synchrotron Radiation Lightsource (SSRL), SLAC National Accelerator Laboratory, is supported by the U.S. DOE, Office of Science, OBES under Contract No. DE-AC02-76SF00515.

The SSRL Structural Molecular Biology Program is supported by the DOE Office of Biological and Environmental Research, and by the National Institutes of Health (NIH), National Institute of General Medical Sciences (NIGMS) (including P41GM103393). The contents of this publication are solely the responsibility of the authors and do not necessarily represent the official views of NIGMS or NIH.

References

- 1 T. W. Clarkson and L. Magos, The toxicology of mercury and its chemical compounds. *Crit. Rev. Toxicol.*, 2006, **36**, 609–662.
- 2 M. Korbas, T. C. MacDonald, I. J. Pickering, G. N. George and P. H. Krone, Chemical form matters: differential accumulation of mercury following inorganic and organic mercury exposures in zebra fish larvae. *ACS Chem. Biol.*, 2012, **7**, 411–420.
- 3 S. Liang, Y. Wang, S. Cinnirella and N. Pirrone, Atmospheric mercury footprints of nations. *Environ. Sci. Technol.*, 2015, **49**, 3566–3574.
- 4 C. T. Driscoll, R. P. Mason, H. M. Chan, D. J. Jacob and N. Pirrone, Mercury as a global pollutant: Sources, pathways, and effects. *Environ. Sci. Technol.*, 2013, **47**, 4967–4983.
- 5 H. H. Harris, I. J. Pickering and G. N. George, The chemical form of mercury in fish. *Science*, 2003, **381**, 1203.
- 6 J. Parížek and I. Ostádalová, The protective effect of small amounts of selenite in sublimate intoxication. *Experientia*, 1967, **23**, 142–143.
- 7 J. Gailer, G. N. George, I. J. Pickering, S. Madden, R. C. Prince, E. Y. Yu, M. B. Denton, H. S. Younis and H. V. Aposhian, The structural basis of the antagonism between inorganic mercury and selenium in mammals. *Chem. Res. Toxicol.*, 2000, **13**, 1135–1142.
- 8 J. Gailer, Arsenic-selenium and mercury-selenium bonds in biology. *Coord. Chem. Rev.*, 2007, **251**, 234–254.
- 9 M. Korbas, J. L. O'Donoghue, G. E. Watson, I. J. Pickering, S. P. Singh, G. J. Myers, T. W. Clarkson and G. N. George, The chemical nature of mercury in human brain following poisoning or environmental exposure. *ACS Chem. Neurosci.*, 2010, **1**, 810–818.

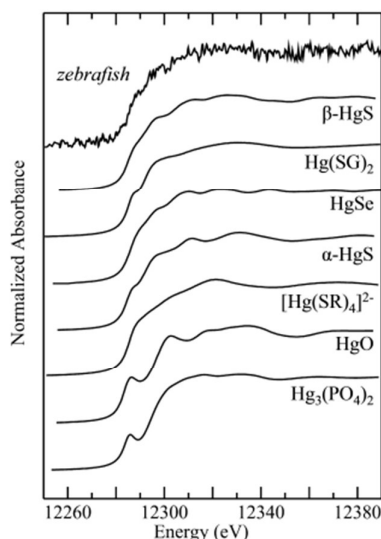


Fig. 9 Hg L_{III} micro X-ray absorption near-edge spectra of zebrafish pronephric duct, compared with spectra of selected model compounds. Data were measured on SSRL 2-3. Best fit comparison between the fish spectrum and individual model spectra gave fit indices ($\times 10^{-3}$) of 1.04 for β -HgS, 1.38 for Hg(SG)₂, 1.42 for HgSe, 1.42 for α -HgS, 1.48 for [Hg(SR)₄]²⁻, 4.44 for HgO and 5.27 for Hg₃(PO₄)₂, indicating that the data are consistent with chalcogenide coordination, and in particular with a substance resembling β -HgS. Hg(SG)₂ and [Hg(SR)₄]²⁻ are aqueous solutions of mercury(II)-bis-S-glutathione and mercury(II)-tetrakis-dimercaptoproanesulfonic acid,³² respectively, both in 50mM HEPES buffer pH 7.0. The fit index is defined as $F = \frac{1}{N-1} \sum_{i=1}^N (d_i - s_i)^2$ where d corresponds to the fish data and s to the standard data, and the summation is over all N data points within the data range of 12260 to 12370 eV.

10 M. Westerfield, *The zebrafish book: a guide for the laboratory use of zebrafish (Brachydanio rerio)*. University of Oregon Press 1995, Eugene OR, ISBN 9994860577

11 M. J. Pushie, I. J. Pickering, M. Korbas, M. J. Hackett and G. N. George, Elemental and chemically specific X-ray fluorescence imaging of biological systems. *Chem. Rev.*, 2014, **114**, 8499–8541.

12 M. Korbas, S. Blechinger, P. H. Krone, I. J. Pickering and G. N. George, Localizing organomercury uptake and accumulation in zebrafish larvae at the tissue and cellular level. *Proc. Natl. Acad. Sci. USA.*, 2008, **105**, 12108–12112.

13 M. Korbas, P. H. Krone, I. J. Pickering and G. N. George, Dynamic accumulation and redistribution of methylmercury in the lens of developing zebrafish embryos and larvae. *J. Biol. Inorg. Chem.*, 2010, **15**, 1137–1145.

14 M. Korbas, B. Lai, S. Vogt, S.-C. Gleber, C. Karunakaran, I. J. Pickering, P. H. Krone and G. N. George, Methylmercury targets photoreceptor outer segments. *ACS Chem. Biol.*, 2013, **8**, 2256–2263.

15 T. C. MacDonald, S. Nehzati, N. J. Sylvain, A. K. James, M. Korbas, S. Caine, I. J. Pickering, G. N. George and P. H. Krone, Phenylthiourea alters toxicity of mercury compounds in zebrafish larvae. *J. Inorg. Biochem.* (submitted)

16 <http://ssrl.slac.stanford.edu/exafspak.html>

17 J. M. Bowness and R. A. Morton, The association of zinc and other metals with melanin and a melanin-protein complex. *Biochem. J.*, 1953, **53**, 620–626.

18 L. Zecca, R. Pietra, C. Goj, C. Mecacci, D. Radice and E. Sabbioni, Iron and other metals in neuromelanin, substantia nigra, and putamen of human brain. *J. Neurochem.*, 1994, **62**, 1097–1101.

19 S. Choudhury, J. K. Thomas, N. J. Sylvain, O. Ponomarenko, R. A. Gordon, S. M. Heald, D. M. Janz, P. H. Krone, I. Coulthard, G. N. George and I. J. Pickering, Selenium preferentially accumulates in the eye lens following embryonic exposure: a

confocal X-ray fluorescence imaging study. *Environ. Sci. Technol.*, 2015, **49**, 2255–2261.

20 S. Krishnan, A. S. Mathuru, C. Kibat, M. Rahman, C. E. Lupton, J. Stewart, A. Claridge-Chang, S. C. Yen and S. Jesuthasan, The right dorsal habenula limits attraction to an odor in zebrafish. *Curr. Biol.*, 2014, **24**, 1167–1175.

21 M. Sakamoto, A. Yasutake, A. Kakita, M. Ryufuku, H. M. Chan, M. Yamamoto, S. Oumi, S. Kobayashi and C. Watanabe, Selenomethionine protects against neuronal degeneration by methylmercury in the developing rat cerebrum. *Env. Sci. Technol.*, 2013, **47**, 2862–2868.

22 M. Yamashita, Y. Yamashita, T. Suzuki, Y. Kani, N. Mizusawa, S. Imamura, K. Takemoto, T. Hara, M. A. Hossain, T. Yabu and K. Touhata, Selenoneine, a novel selenium-containing compound, mediates detoxification mechanisms against methylmercury accumulation and toxicity in zebrafish embryo. *Mar. Biotechnol.*, 2013, **15**, 559–570.

23 S. Yoneda and K. T. Suzuki, Equimolar Hg-Se complex binds selenoprotein P. *Biochem. Biophys. Res. Commun.*, 1997, **231**, 7–11.

24 K. T. Suzuki, C. Sasakura and S. Yoneda, Binding sites for the (Hg-Se) complex on selenoprotein P. *Biochim. Biophys. Acta*, 1998, **1429**, 102–112.

25 A. Nakayama, K. E. Hill, L. M. Austin, A. K. Motley and R. F. Burk, All regions of mouse brain are dependent on selenoprotein P for maintenance of selenium. *J. Nutr.*, 2007, **137**, 690–693.

26 K. E. Hill, S. Wu, A. K. Motley, T. D. Stevenson, V. P. Winfrey, M. R. Capocchi, J. F. Atkins and R. F. Burk, Production of selenoprotein P (Sepp1) by hepatocytes is central to selenium homeostasis. *J. Biol. Chem.*, 2012, **287**, 40414–40424.

27 W. F. de Jong, Die Struktur des Tiemannit und Coloradoit. *Z. Kristallogr.*, 1926, **63**, 466–472.

28 J. W. Earley, Description and syntheses of the selenide minerals. *Am. Mineral.*, 1950, **35**, 337–364.

29 H. E. Buckley and W. S. Vernon, The crystal structures of the sulfides of mercury. *Mineral. Mag. J. M. Soc.*, 1925, **20**, 382–392.

30 N. Z. Boctor, J. B. Brady, Interdiffusion of sulfur and selenium in tiemannite. *Amer. Mineral.*, 1980, **65**, 797–799.

31 M. Kuno, K. A. Higginson, S. B. Qadri, M. Yousuf, S. H. Lee, B. L. Davis and H. Mattoussi, Molecular clusters of binary and ternary mercury chalcogenides: colloidal synthesis, characterization, and optical spectra. *J. Phys. Chem. B*, 2003, **107**, 5758–5767.

32 G. N. George, R. C. Prince, J. Gailer, G. A. Buttigieg, M. B. Denton, H. H. Harris and I. J. Pickering, Mercury binding to the chelation therapy agents DMSA and DMPS, and the rational design of custom chelators for mercury. *Chem. Res. Toxicol.* 2004, **17**, 999–1006.

33 G. N. George, S. P. Singh, R. C. Prince and I. J. Pickering, The chemical forms of mercury and selenium in fish following digestion with simulated gastric fluid. *Chem. Res. Toxicol.*, 2008, **21**, 2106–2110.

34 A. Drott, E. Björn, S. Bouchet and U. Skyllberg, Refining thermodynamic constants for mercury(II)-sulfides in equilibrium with metacinnabar at sub-micromolar aqueous sulfide concentrations. *Environ. Sci. Technol.*, 2013, **47**, 4197–4203.

35 C. M. Weekley and H. H. Harris, Which form is that? The importance of selenium speciation and metabolism in the prevention and treatment of disease. *Chem. Soc. Rev.*, 2013, **42**, 8870–8894.

36 N. V. C. Ralston, J. L. Blackwell III and L. J. Raymond, Importance of molar ratios in selenium-dependent protection against methylmercury toxicity. *Biol. Trace Elem. Res.*, 2007, **119**, 255–268.